View metadata, citation and similar papers at core.ac.uk
brought to you by CORE
provided by Servicio de Coordinación de Bibliotecas de la Universidad Politécnica de Madrid

Aluminium Nitride Solidly Mounted BAW Resonators with Iridium Electrodes

Marta Clement, Jimena Olivares, Enrique Iborra, Sheila González-Castilla, Jesús Sangrador, *Grupo de Microsistemas y Materiales Electrónicos, Universidad Politécnica de Madrid, Spain*
Nick Rimmer, Amit Rastogi, *Aviza Tecnology Inc. Newport, South Wales, UK*
Brice Ivira, Alexandre Reinhardt, *CEA-Leti Minatec, Grenoble, France*

ABSTRACT

In this work we investigated the performance of aluminium nitride (AlN)-based solidly mounted resonators (SMR) made with iridium (Ir) bottom electrodes. Ir/AlN/metal stacks were grown on top of insulating Bragg mirrors composed of alternate λ/4 layers of silicon oxi-carbide (SiOC) and silicon nitride (Si_3N_4). Ir electrodes of various thicknesses were electron-beam evaporated on different adhesion layers, which also acted as seed layers. AlN was deposited by sputtering after conditioning the Ir electrode by a soft-etch with Ar^+ ions, which was essential to achieve high quality AlN films. The structure and morphology of the different layers were analysed by x-ray diffraction (XRD) and atomic force microscopy (AFM). The frequency response of the SMRs was assessed by measuring the input scattering parameter S_{11} with a network analyzer. The experimental results were fitted to the Butterworth-Van Dyke circuital model. The effective electromechanical coupling factor k^2_{eff}, and the quality factor Q of the resonators were derived from the experimental data. The influence of the thickness, crystal quality and roughness of the Ir bottom electrodes on the performance of the resonators was investigated.

INTRODUCTION

High frequency oscillators and filters in the GHz band based on bulk acoustic wave (BAW) resonators are currently in great demand owing to the rapid growth of wireless communications systems. The recent advances in the sputtering of piezoelectric AlN thin films, fully compatible with conventional silicon technologies, has allowed the industrialization of AlN-based BAW filters [1, 2]. Two configurations are typically used to enhance the mechanical isolation of the acoustic wave: the suspended film bulk acoustic resonator (FBAR) [3] and the solidly mounted resonator (SMR) [4], the latter being the more suitable for integration and high power handling [5].

A SMR consists of a piezoelectric thin film sandwiched between two thin electrodes built on top of an acoustic mirror, called a Bragg reflector. The Bragg reflector consists of a sequence of a-quarter-wavelength-thick layers of low and high acoustic impedance. At each layer interface of the Bragg reflector, a part of the acoustic wave energy is reflected. The number of layers in the Bragg reflector needed for complete wave reflection is determined by their acoustic impedance ratio. Typically, high impedance layers are fabricated from tungsten (W), molybdenum (Mo), tantalum oxide (Ta_2O_5) or aluminium nitride (AlN), and the low impedance layer from silicon dioxide (SiO_2) or aluminium (Al). Depending on the nature of the two layers, one can obtain fully conductive Bragg mirrors [6], fully insulating mirrors [7], or mixed reflectors [8].

Many efforts are devoted to improve the performance of SMRs through the investigation of new materials and device configurations allowing to reduce the piezoelectric losses and to increase the power handling capacity. The choice of the bottom electrode is an especially sensitive task, as this material takes an active part in many aspects of the device performance. The first requirement is its ability to promote the growth of highly *c*-axis oriented AlN films exhibiting a single polar orientation, to guarantee a high piezoelectric activity; nucleation surfaces exhibiting well-defined hexagonal symmetry seems to be the key issue to start the growth of high quality (00·2)-oriented AlN [7]. Additionally, smooth [9] and highly-textured [10] nucleation substrates provide films of higher crystal quality. Other factors that contribute to further improve the crystalline properties of AlN are, for example, the use of seed layers under the metal electrode [11], the pre-conditioning of the nucleation surface by an in-situ ion etch before AlN deposition [12], and of course, the comprehensive choice of the sputter parameters [13]. The metallic electrodes should also contribute to the confinement of the mechanical energy in the piezoelectric layer by providing a large impedance mismatch with AlN; heavy and stiff metals are the candidates of choice [14]. Other considerations for the selection of the appropriate electrode are its thermal and chemical stabilities, price and compatibility with conventional silicon technologies.

Metals most frequently used in BAW applications are W [15], Pt [4], Mo [16], although many others (Al, Ta, Ti, Cu, Cr, Au, Ru) have been investigated [14, 17]. So far, the best-textured AlN films deposited by sputtering on metallic surfaces have been grown on Pt substrates, with values of the full width at half maximum (FWHM) of the rocking-curve (RC) around the 00·2 peak of around 0.9º for 2 μm-thick films [7]. Iridium (Ir) is a precious metal similar to Pt although considerably cheaper. Like Pt, Ir crystallizes in the (fcc) structure, in which the {111} planes exhibit hexagonal symmetry, thus offering

an appropriate surface for the nucleation of *c*-axis oriented AlN. Additionally, Ir possesses a very high acoustic impedance, as a result of its high density (22.5 $g\cdot cm^{-3}$) and high sound velocity (5300 m/s). Finally, regarding the compatibility with CMOS technology, it is worth noting that Ir diffusivity in Si is considerably lower than that of other heavy metals (Au, Pt) and its activity as a recombination centre is only significant at high injection levels [18]. It has been demonstrated recently [19] that Ir indeed favours the growth highly oriented AlN films. Besides, a preliminary assessment of Ir-based test resonators fabricated on poorly isolated structures predicted a good performance in operative devices [20].

The aim of this work was to investigate the viability of using Ir as bottom electrode in operative AlN-based SMRs. Mo/AlN/Ir stacks were grown on top of insulating Bragg mirrors to obtain resonators with a good acoustic isolation. We report first the structural characterization of the different layers and analyze the influence of the Ir deposition process in the crystal quality of the AlN films. We investigate then the influence of the thickness, crystal quality and roughness of the Ir bottom electrodes on the performance of the SMRs built on acoustic reflectors.

EXPERIMENTAL DETAILS

Mo/AlN/Ir stacks were grown on two sets of Bragg mirrors formed by alternating low and high acoustic impedance layers of SiOC (3.6×10^6 $N\cdot s\cdot m^{-3}$) and Si_3N_4 (25.7×10^6 $N\cdot s\cdot m^{-3}$), respectively. The first set of mirrors consisted of two pairs of SiOC and Si_3N_4. The second set contained three pairs of layers and was terminated by a low-roughness SiO_2 layer. In all cases, an all-insulating acoustic reflector was achieved.

Different sputtered seed layers were used to improve the adhesion and crystal quality of the Ir bottom electrode to the acoustic reflector. These consisted of 20 nm-thick Ti films or Mo/Ti bilayers, 20 nm-thick Mo/AlN bilayers, and 40 nm-thick Mo/AlN bilayers. Ir slugs (99.98% pure) were electron-beam evaporated at a base pressure of 1×10^{-6} Torr to form bottom electrodes of different thicknesses. Before deposition, the Ir slugs were red-hot heated until the selected deposition rate was reached; this warm-up also cleaned the surface of the Ir slugs. Ir layers were then evaporated to a thickness of 100 nm to 300 nm by opening a mechanical shutter.

AlN piezoelectric films were reactively sputtered with a pulsed DC source in a Sigma fxP cluster tool from Aviza Technology (see Fig. 1). Before AlN deposition a conditioning process of the Ir bottom electrode by a 15 s soft-etch with Ar^+ ions was performed. A dedicated heat station was used to degas the wafer close to the AlN deposition temperature. AlN films were sputtered with a 1:5 Ar/N_2 admixture at a total pressure of 5 mTorr, a pulsed DC power level of 10 kW, and a platen temperature of 400ºC. An RF bias was applied to the substrates to tune the stress in the AlN films to 0±50MPa. These conditions provided deposition rates of 100 nm/min with in-wafer thickness homogeneity of 0.3%. Mo top electrodes were then deposited and patterned by dry-etching in SF_6. Finally, the AlN film was wet-etched in a KOH solution to reach the iridium bottom electrode.

Figure 1. Sputtering tool used for the deposition of AlN films

The crystal structure of the Ir and AlN films was assessed by X-ray diffraction (XRD) by measuring the θ/2θ patterns and the rocking-curves (RC) around the most intense reflections, i.e. the AlN 00·2 at 18.02º(θ) and the Ir 111 at 20.35º(θ). The surface of the different layers was examined by atomic force microscopy (AFM), which provided the measurement of the surface roughness.

The resonators were characterized by measuring the electrical reflection coefficient (S_{11}) at frequencies ranging from 30 kHz to 3 GHz, using an Agilent 8753ES network analyzer connected to the samples through a coplanar RF probe from Picoprobe Inc.

RESULTS AND DISCUSSION

Material structure

The crystal quality of AlN films depends significantly on the sputter parameters (gas composition, total pressure, substrate temperature, RF power and substrate bias). Optimization of the deposition conditions is thus essential to achieve good material characteristics, although not sufficient, as other factors, such as the nature and crystal quality of the bottom electrode or its pretreatment before AlN deposition, are also key factors to obtain high quality material. We have shown in a previous work [19] that the growth of (111)-oriented Ir films can be favoured by using adequate seed layers (Ti or Mo/Ti), substrate temperatures of around 400ºC and low roughness substrates. Besides, the crystal quality of AlN films sputtered on Ir electrodes tends to improve slightly with the texture of the Ir films and is clearly enhanced after a conditioning of the Ir surface by a soft bombardment with Ar^+ ions.

In this work, we have observed a certain influence of the nature of the different seed layers investigated (Ti (20 nm), Ti/Mo (20/40 nm), AlN/Mo (15/20-40 nm)) on the crystal quality of the subsequently deposited Ir films. Generally speaking, Ti/Mo seed layers seemed to promote the growth of the best-oriented Ir films, followed by Ti seed layers. AlN/Mo bilayers yielded the Ir films of poorer crystal quality (although most of the films

investigated were highly *c*-axis oriented). However, it is important to point out that the seed layers investigated here were deposited under different sputter conditions in different systems; besides, some of them were exposed to ambient for long periods. Therefore, definite conclusions cannot be drawn.

To achieve AlN *c*-axis-oriented films on (111)-oriented Ir surfaces a soft etch of the Ir surface with Ar^+ ions before the AlN deposition was required. This bombardment was carried out during 15 s with an Ar glow discharge at high pressure (1 Torr). The substrates were kept at a low bias voltage (below 100 V). This pretreatment of the Ir surface guaranteed the growth of AlN films of pure (00·2) orientation [19]. Figure 2 shows the XRD patterns of AlN films grown on Ir surfaces with and without Ar^+ pretreatment. Reflections of AlN and Ir can be observed. Most of the XRD patterns exhibited a small peak at θ=23.7º corresponding to the Ir (200) reflection in addition to the Ir (111) one, revealing the existence of non (111)-oriented grains.

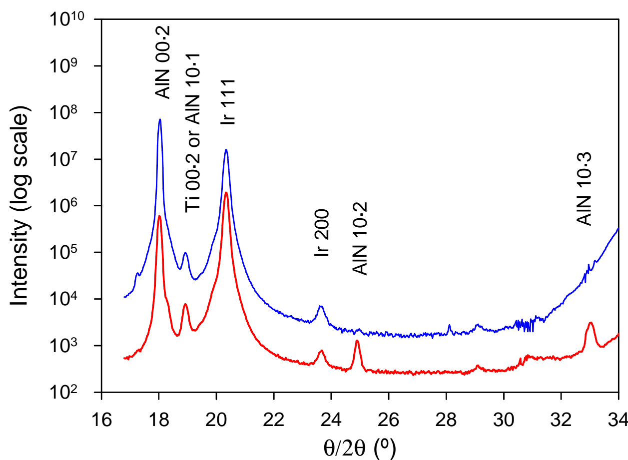

Figure 2. XRD patterns of AlN films on pretreated Ir films (top trace) and non-pretreated Ir films (bottom trace). (Top trace was shifted for clarity).

The effect of the soft etch on the surface of the Ir layer is not well understood. However, it produced a clear effect in the orientation of the AlN film. If this was omitted, the XRD measurements of the films exhibited, in addition to the large (00·2) peak, traces of (10·1), (10·2), and (10·3) reflections, revealing the presence of a significant amount of tilted grains in a matrix of *c*-axis oriented grains. Additionally, the FWHM of the RC around the AlN (00·2) reflection was high (up to 8º). After the soft etch of the Ir surface all the reflections others than the (00·2) disappeared; this effect was accompanied by a significant narrowing of the RC. A possible explanation of the effect of the soft etch could be a uniform generation of nucleation centres, which promoted the growth of (00·2) oriented AlN, although further investigations are required to explain the effect of the soft etch. In this work, only purely *c*-axis-oriented AlN films deposited on preconditioned Ir layers were used to fabricate the SMRs.

We investigated then the influence of the roughness of the available Bragg reflectors in the crystalline structure of both the evaporated Ir films and the sputtered AlN films. Fig.3 shows two AFM images of the Bragg mirrors along with the horizontal cross section of their surface. We observe that Bragg mirrors terminated with a SiOC layer (Fig. 2a) were significantly rougher than those terminated with a SiO_2 layer (Fig. 2b).

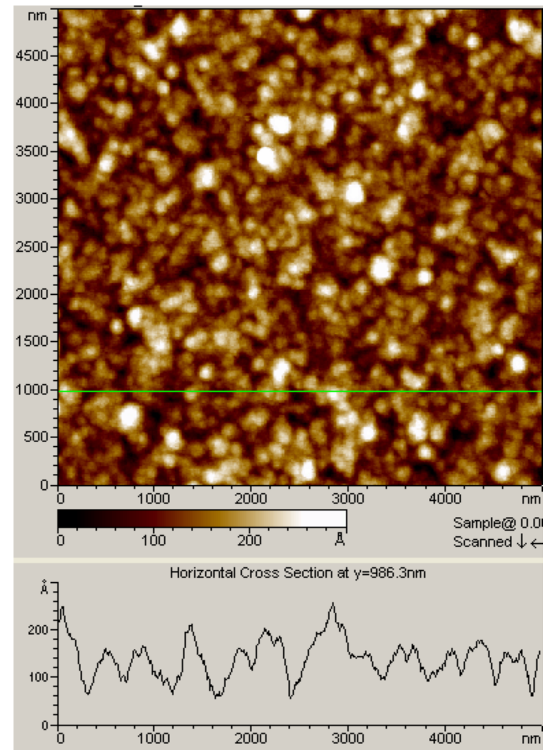

(a)

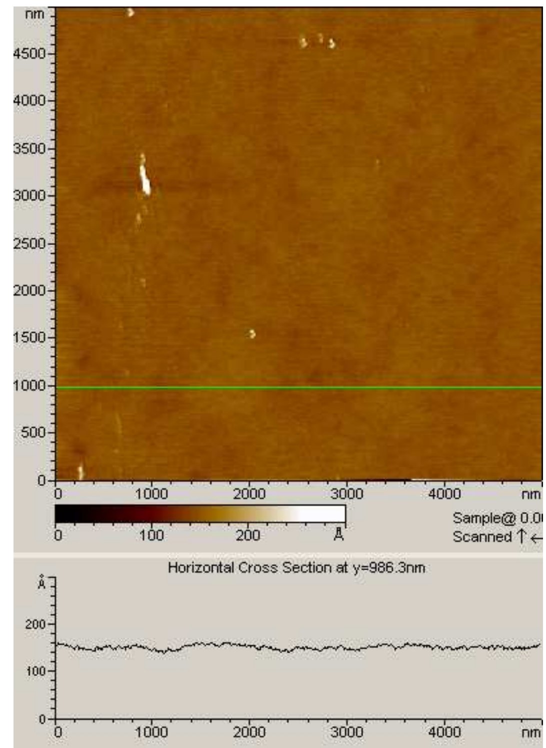

(b)

Figure 3. AFM images of the surface of Bragg mirrors terminated with (a) SIOC layer and (b) SiO_2 layer.

The influence of Bragg mirrors roughness on the crystal structure of the subsequent Ir layers was significant. The full width at half maximum (FWHM) of the RC around of the Ir (111) reflection was around 9º for the rough surface, whereas it narrowed to 4º for the smoother surface.

However, the influence of the roughness on the crystal structure of the AlN films was significantly weaker. Fig. 4 shows the AFM images of the surface of AlN films grown on a rough (Fig. 4a) and a smooth (Fig. 4b) Bragg mirror, respectively.

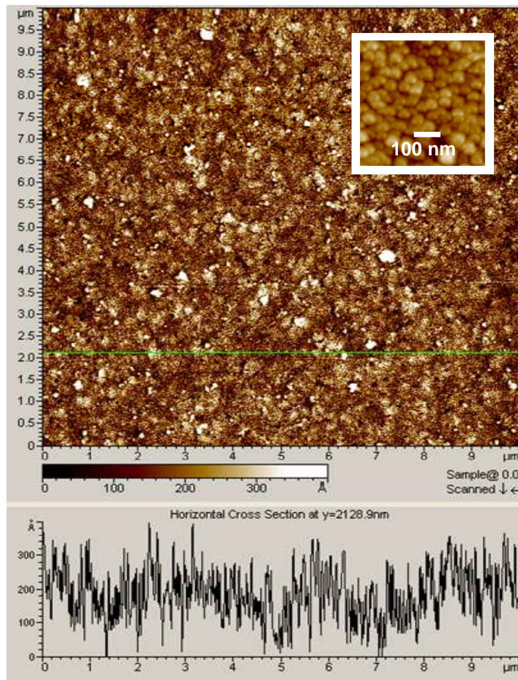

(a)

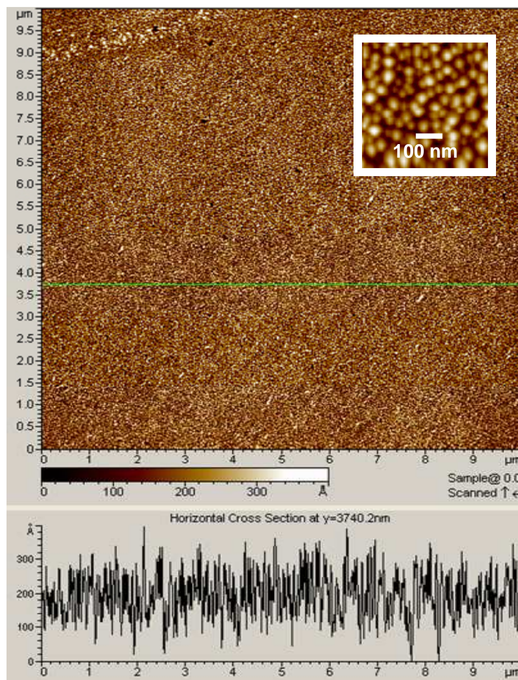

(b)

Figure 4. AFM images of the surface of AlN films deposited on (a) a rough Bragg mirror and (b) on a smooth Bragg mirror.

Fig. 4a shows that the long-range roughness of the underlying substrate was clearly transferred to the AlN film; however, this did not seem to affect significantly the growth of *c*-axis oriented columnar grains. The image reveals a short-range grainy film surface (the rounded grains correspond to the top of the columns normal to the surface), similar to that of AlN films grown on smooth surfaces (Fig. 4b). A closer view of the grainy structure (see the insets) reveals that the mean basal diameter of the grains was around 50 nm to 60 nm for both films.

The XRD patterns of the layers (Ir and AlN) grown on different substrates confirmed the results exposed previously. Fig. 5 shows the FWHM of the RC around the AlN (00·2) peak as a function of the FWHM of the RC around the Ir (111) peak, for some AlN/Ir bilayers grown on a great variety of substrates, which included the use different reflector stacks and different seed layers. The Ir surface of all the samples was always soft etched. The most interesting conclusion derived from data of Fig.5 is that the growth of highly textured AlN films was weakly dependent on the texture of the underlying Ir layer. For example, Ir layers evaporated on rough Bragg mirrors and exhibiting a poor 111 texture (RC values between 8º and 10º) could promote, however, the growth of well (00·2)-textured AlN films (RC around 2º). It is important to note that actually, the use substrates of different roughness covered with seed layers of different nature and thickness significantly affected the crystal quality of the evaporated Ir, which exhibited RC varying from 3.8º for the best textured films to 10.5º. However, the RC of the AlN films remained below 3.8º, reaching values as low as 0.9º for the best films. This suggests that the changes undergone by the Ir surface as a consequence of the Ar^{+} bombardment were far more significant for the growth of oriented AlN than the original texture of the layer. Other factor influencing the width of the AlN RC was the thickness of the film, as thicker AlN films exhibited narrower RCs.

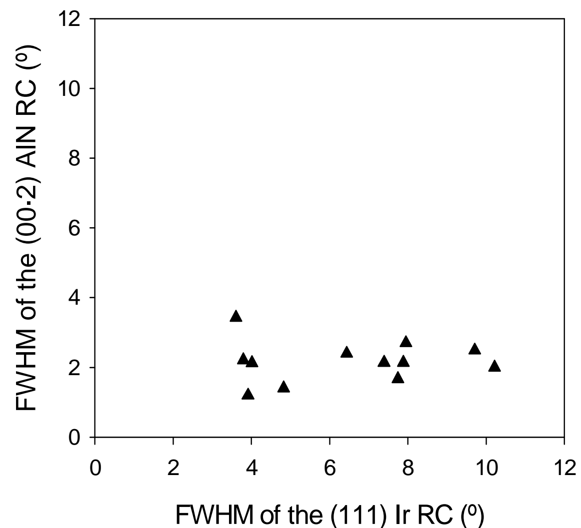

Figure 5. FWHM of the RC around AlN 00·2 peak vs. FWHM of the RC around Ir 111 peak for AlN/Ir bilayers grown on different substrates.

Assessment of BAW resonators

The thickness of the Ir bottom electrode and the AlN piezoelectric layer were adjusted to obtain SRMs of similar resonant frequency, so that resonators with thicker Ir bottom electrodes required thinner AlN layers. The thickness of the Ir bottom electrode was varied between 85 nm and 260 nm; correspondingly, the thickness of the AlN films was varied between 1600 nm and 1100 nm values, which provided resonant frequencies of

approximately 2.05 GHz. The upper electrode was identical for all the devices and consisted of a 180 nm-thick Mo layer.

The response of the resonators was assessed by measuring the electrical reflection coefficient S_{11} at frequencies ranging from 30 kHz to 3 GHz. Fig.6 shows the frequency variation of the modulus and the phase of the complex impedance of a representative resonator.

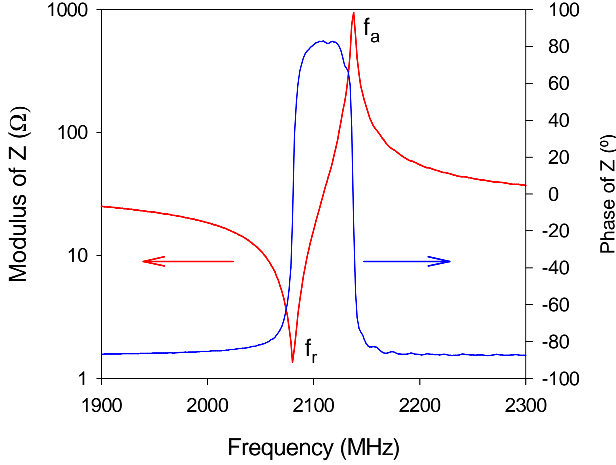

Figure 6. Measured values of the frequency variation of the complex impedance (modulus and phase) of a representative resonator.

The effective coupling factor of the SMRs k^2_{eff} (using the standard definition of IEEE [1]) was obtained from values of the resonant (f_r) and antiresonant (f_a) frequencies, through the expression

$$k_{eff}^2 = \frac{\pi}{2}\frac{f_r}{f_a}\frac{1}{\tan\left(\frac{\pi}{2}\frac{f_r}{f_a}\right)} \quad (1)$$

The resonant and antiresonant quality factors ($Q_{r,a}$) were derived from the slope of curve of the impedance phase versus frequency at the resonant and antiresonant frequencies, respectively [1].

$$Q_{r,a} = \frac{f_{r,a}}{2}\left(\frac{d\angle Z}{df}\right)_{f_{r,a}} \quad (2)$$

The experimental data were fitted with the modified Butterworth Van Dyke (BVD) circuital model [21] of Fig. 7 to determine the values of the lumped elements describing the resonator behaviour. A second definition of the quality factor was obtained from the values of the lumped components through the expression

$$Q_c = \frac{1}{2\cdot\pi\cdot f_r\cdot R_m\cdot C_m} \quad (3)$$

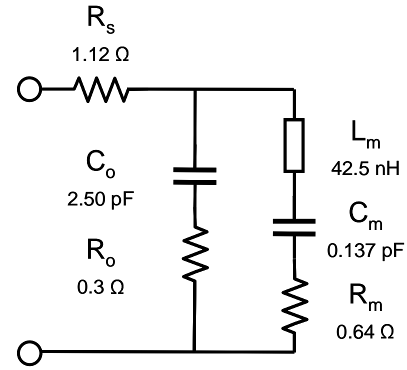

Figure 7. Modified Butterworth Van Dyke model with the values of the lumped elements obtained for the resonator of figure 6.

The values of the effective coupling factor k^2_{eff} measured in all the devices under study have been depicted in Fig. 8 as a function of the FWHM of the RC around of the AlN (00·2) peak, considering the latter as indicative of the crystal quality of the piezoelectric film.

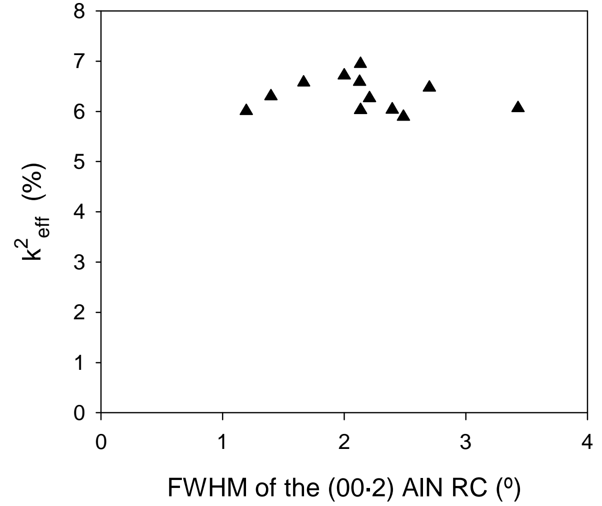

Figure 8. Electromechanical coupling factor of several resonators vs. the FWHM of the RC around the AlN (00·2) reflection.

Data of Fig. 8 show that k^2_{eff} ranged between 6% and 7%, which reveals that AlN films grown on Ir bottom electrodes exhibited significantly high piezoelectric responses. Besides, the values of k^2_{eff} were rather independent of the FWHM of the RC around the AlN (00·2) reflection, contrary to what is generally assumed. This result suggests that AlN films grown on Ir surfaces were relatively free of the electrically active defects that degrade their piezoelectric response. Actually, the crystal defects that degrade the piezoelectric response more severely are those related to the existence of grains with opposite polar orientation (frequently present in layers of bad crystal quality, such as those grown on non-etched Ir substrates), but that do not necessarily produce a widening of the RC. A widening of the RC by a few degrees should only reduce the piezoelectric response by a geometrical factor slightly lower than 1, which can be estimated by integrating, over the tilt angle, the projection of the polarization vector on the electric field direction [22].

The dispersion of the values of k^2_{eff} is attributed to the use of substrates of different nature and roughness

leading to Ir layers of different crystal quality (width of the RC), which in turn slightly affected the AlN quality (see figure 5) and, obviously, to the different thicknesses of the Ir electrode and AlN layer. No clear trend in the variation of k^2_{eff} with any other variable tested was observed. Generally speaking, smooth substrates and highly (111) textured Ir films with narrow RC provided resonators with the highest coupling factors.

The influence of the thicknesses of the Ir electrode and AlN layer in the performance of the SMRs was also investigated. Fig. 9 shows the measured values of k^2_{eff} as a function of the ratio of the thicknesses of the Ir bottom electrode and the piezoelectric AlN for a set of resonators made on smooth substrates. The theoretical variation of k^2_{eff} using the one dimension Mason's model [23] is also depicted for comparison. It is important to remind that the thicknesses of the layers were adjusted to achieve a resonant frequency close to 2.05 GHz.

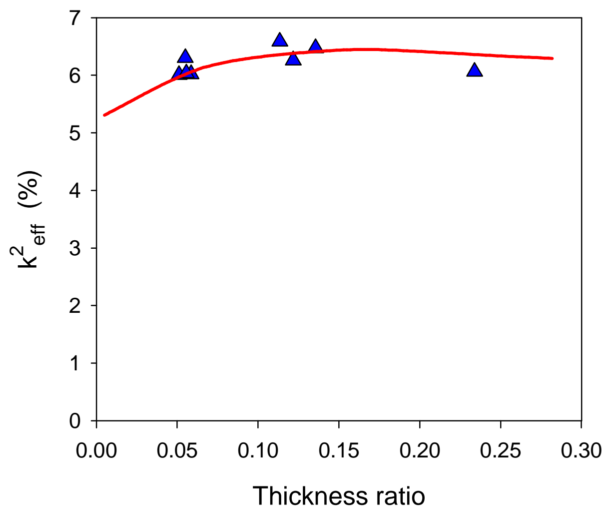

Figure 9. k^2_{eff} as a function of the thickness ratio (Ir/AlN) for several SMRs built on smooth Bragg mirrors. Solid line is the simulation using Mason's model.

Mason´s model predicts that the variation of k^2_{eff} with the thickness ratio (Ir/AlN) exhibits a maximum, whose position and intensity are related with the acoustic impedance mismatch between the two materials. This effect has been previously studied for some metallic electrodes, such as Al, Au, Mo, and W [24-26]. In the case of Ir, the variation of k^2_{eff} was very smooth, similar that observed in Mo or W-based SMRs, due to the large acoustic impedance mismatch between the metal electrode (Ir, Mo, or W) and AlN. A different behaviour was observed for metals of acoustic impedance closer to that of AlN, such as gold, where a stronger variation of k^2_{eff} with the thickness ratio appeared. This behaviour is undesirable as it limits the flexibility in the design of the devices.

The other magnitude used to evaluate the quality of the resonators is the quality factor Q. This magnitude is a relative measurement of the energy not confined in the resonator, which has been lost by different mechanisms. These losses can be electrical, due to the dissipation in the materials (metals and dielectrics), or mechanical, due to mechanical energy lost through the substrate or out of the resonators through shear modes propagating parallel to the surface. In the practice, there is not a general theory accounting for the behaviour of the quality factor, as there is not a clear criterion to calculate it either. For the devices presented here, the quality factor depends strongly on the definition considered, as we can observe in Fig. 10, where the three values Q_r, Q_a and Q_c derived from equations (2) and (3) are depicted as a function of the AlN RC (the solid lines are only a guide for the eyes).

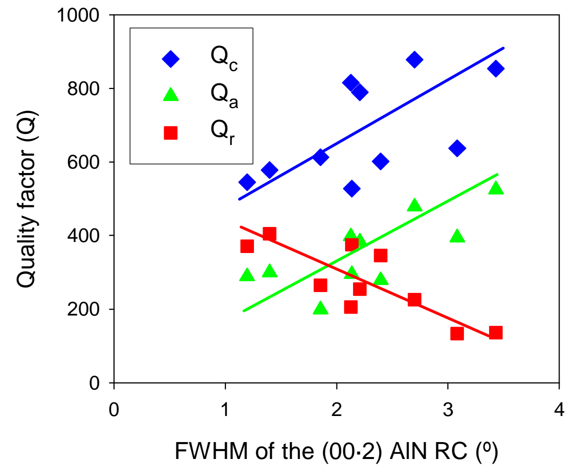

Figure 9. Q_r (■), Q_a (▲) and Q_c (♦) (from eq. 2 and eq. 3) as a function of the RC around AlN (00·2) reflection. Lines are only for guiding.

The opposite variation of the resonant (Q_r) and antiresonant (Q_a) quality factors suggests the existence of loss mechanisms of different nature, which should be investigated in depth with additional experiments. Q_c derived from the BVD model was always higher than Q_r and Q_a, because the former only considers the series resistance of the motional arm of the BVD model (R_m in figure 7), disregarding the effect of the electrical losses represented by R_s and R_0. Similar variations of Q_r and Q_a have been reported [27], but we have not found in the literature an explanation for this behaviour.

CONCLUSIONS

A new material, Ir, is proposed as bottom electrode in AlN-based SMRs. BAW resonators composed of a Mo/AlN/Ir stacks deposited on SiCO/SiN Bragg mirrors were fabricated. The thickness of the Ir and AlN films were varied simultaneously to achieve a resonant frequency of 2.05 GHz in all the devices. The overall quality of the materials composing the piezoelectric capacitor (Ir and AlN) was optimized by using low roughness Bragg mirrors, Ti or Mo/Ti seed layers to enhance the adhesion of Ir to the Bragg reflector, and by pretreating the Ir surface with Ar^+ ions before AlN deposition. Under these conditions, AlN films of good crystal quality were successfully grown, almost independent of the texture and roughness of the underlying Ir electrode. The analysis of the frequency response of SMRs revealed the high piezoelectric activity of AlN grown on Ir electrodes. Effective coupling factors (k^2_{eff}) ranging from 6% to 7% and almost independent of the FWHM of the RC around the AlN 00·2 reflection and

Ir/AlN thickness ratios were obtained, confirming the suitability of Ir as bottom electrode in SMRs. The quality factor Q_c derived from the BVD circuital mode reached values close to 1000. However, the measured resonant (Q_r) and antiresonant (Q_a) quality factors were lower and exhibited an opposite behaviour with the width of RC of AlN, which should be investigated in the near future.

ACKNOWLEDGMENT

This work was partially supported by the European Commission through the 6th Framework Program by the MOBILIS project. (http://www.ist-mobilis.org)

REFERENCES

1. R. Aigner, Proc 3rd Int Symposium on Acoustic Wave Devices for Future Mobile Communication Systems, Chiba, Japan, Mar.(2007).
2. E. Schmidhammer, H. Heinze, M. Schmiedgen, M. Mayer, and A. Link, IEEE Ultrason. Symp. Proc., 329 (2006).
3. K.M. Lakin, IEEE FCS-EFTF Proc. 1 (2003).
4. H.P. Loebl, M. Klee, C. Metzmacher, W. Brand, R. Milsomb, and P. Lokc, Mat. Chem. and Phys. 79, 143 (2003).
5. R. Aigner, N-H. Huynh, M. Handtmann, and S. Marksteiner, IEEE Ultrason. Symp. Proc., 429 (2005).
6. J. Enlund, D. Martin, V. Yantchev and I. Katardjiev, Sen. Actuators A, 141(2), 598 (2008).
7. R. Lanz and P. Muralt, IEEE Trans. Ultrason. Ferr. Freq. Control, 52 (6), 936 (2005).
8. C-J. Chung, Y-C Chen, C-C Cheng, and K-S Kao, Thin Solid Films (2007), doi:10.1016/j.tsf.2007.07.050.
9. Guoqiang Li, Tae-Won Kim, Shigeru Inoue, Koichiro Okamoto, and Hiroshi Fujioka, Appl. Phys. Lett. **89**, 241905 (2006).
10. R. Jakkaraju, G. Henn, C. Shearer, M. Harris, N. Rimmer, and P. Rich, Microelec. Eng. 70, 566 (2003).
11. T. Kamohara, M. Akiyama, N.Ueno, K. Nonaka, N. Kuwano, Thin Solid Films 515, 4565 (2007).
12. B. Paci, A. Generosi, V. Rossi. M. Benetti, D. Cannatà, F. Pietrantonio and E. Verona, Sens. Actuators A 137, 279 (2007).
13. M. Clement, E. Iborra, J. Sangrador, A. Sanz-Hervás, L. Vergara, M. Aguilar, J. Appl. Phys. 94, 1495 (2003).
14. T. Yokoyama, T. Nishihara, S. Taniguchi, M. Iwaki, Y Satoh, M. Ueda, and T. Miyashita, IEEE Ultrason. Ferr. Freq. Control Proc. 429 (2004).
15. E. Schimdhammer, B. Bader, W. Sauer, M. Schmiedgen, H. Heinze, C. Eggs, and T. Metzger, Microw. Symp. Digest IEEE MTT-S Proc. 233 (2005).
16. Y-R. Kang, S-C. Kang, K-K. Paek, Y-K. Kim, S-W. Kim and B-K. Ju, Sens. Actuators A 117, 62 (2005).
17. M. Akiyama, K. Nagao, N. Ueno, H. Tateyama, T.Yamada, Vacuum 74, 699 (2004).
18. V. Benda, M. Cernik and D. Stepkova, Microel. J., 29, 695 (1998).
19. J. Olivares, M. Clement, E. Iborra, S. González-Castilla, N. Rimmer and A. Rastogi, IEEE Ultrason. Symp. Proc., 1401 (2007).
20. E. Iborra, M. Clement, J. Olivares, J. Sangrador, N. Rimmer and A. Rastogi, IEEE Ultrason. Symp. Proc., 616 (2007).
21. J. Larson, P.Bradley, S. Wartenberg, R.Rudy, IEEE Ultrason. Symp. Proc. 863 (2000).
22. S. Mishin, D. R. Marx, and B. Sylvia, IEEE Ultrason. Symp. Proc., 2028 (2005).
23. J. Rosenbaum, Dec. 1945, reprinted by Artech House, Boston (1988).
24. A. Reinhardt, V. Laude, Th. Pastureaud, S. Ballandras, IEEE Ultrason. Symp. Proc., 497 (2002).
25. K.M. Lakin, J.Belsick, J.F. McDonald, and K.T. McCarron, IEEE Ultrason. Symp. Proc., 827 (2001).
26. Q. Chen and Q.M. Wang, Appl. Phys. Lett, 86, 022904 (2005).
27. C.L. Huang, K.W. Tay, and L.Wu, Jap. J. Appl. Phys., 44, 1397 (2005).